

Invited review to appear in XVIIth Moriond Astrophysics Meeting: Extragalactic Astronomy in the INFRARED, les Arcs, France, March 1997, ed. G.A. Mamon, T.X. Thuan & J. Tran Thanh Van (Paris: Frontières)

Galaxies and Cosmology with DENIS

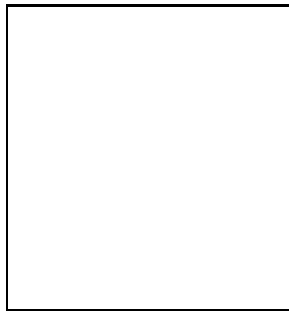
G.A. Mamon ^{1,2}, M. Tricottet ¹, W. Bonin ^{1,3}, V. Banchet ^{1,4},

¹ Institut d'Astrophysique, Paris, France.

² DAEC, Observatoire de Paris, Meudon, France.

³ Université Paris XI, Orsay, France.

⁴ CYBEL, SA, Paris, France.



Abstract

The DENIS survey is currently imaging 21334 deg² of the mainly southern sky in the *IJK* and the observations are expected to go on until mid 2000. The expectations for extragalactic and cosmological research are outlined, including a quantitative assessment of the effects of recent star formation on the measured fluxes of galaxies. The galaxy extraction is much improved with the modeling of the PSF across the 12' × 12' frames and the reliability of star/galaxy separation (currently based upon a combination of classical and neural-network based methods) is measured from visual inspection to be > 90% at *I* = 16. The *I* band counts follow the high bright-end normalization and the *J* differential counts follow $N(J) \simeq 11 \times \text{dex}[0.6(J - 14)] \text{ deg}^{-2} \text{ mag}^{-1}$ and are expected to be complete, reliable and photometrically accurate ($\Delta m < 0.1$) for $J \leq 14$.

1 Cosmology and Near-Infrared selection

Workers in the Infrared bands know that the Near-Infrared (NIR) is 4 (*J*) to 10 (*K*) times less affected by extinction from dust than is the *V* band [9]. This has two advantages: 1) A nearly-full view of the Universe, even behind the Zone of Avoidance, and 2) A view of external galaxies unaffected by their internal extinction by dust.

The second advantage of the Near-Infrared is its smaller bias to recent star formation, in comparison with bluer bands and also to the mid and far IR, whose emission arises from thermal dust created and heated by young stars.

The lack of sensitivity to recent star formation can be quantified as follows. Figure 1 shows the evolution of broad-band luminosities, normalized to that of a 13 Gyr old stellar population for different color bands. The evolution is strongest in the *B* band (and even more so in

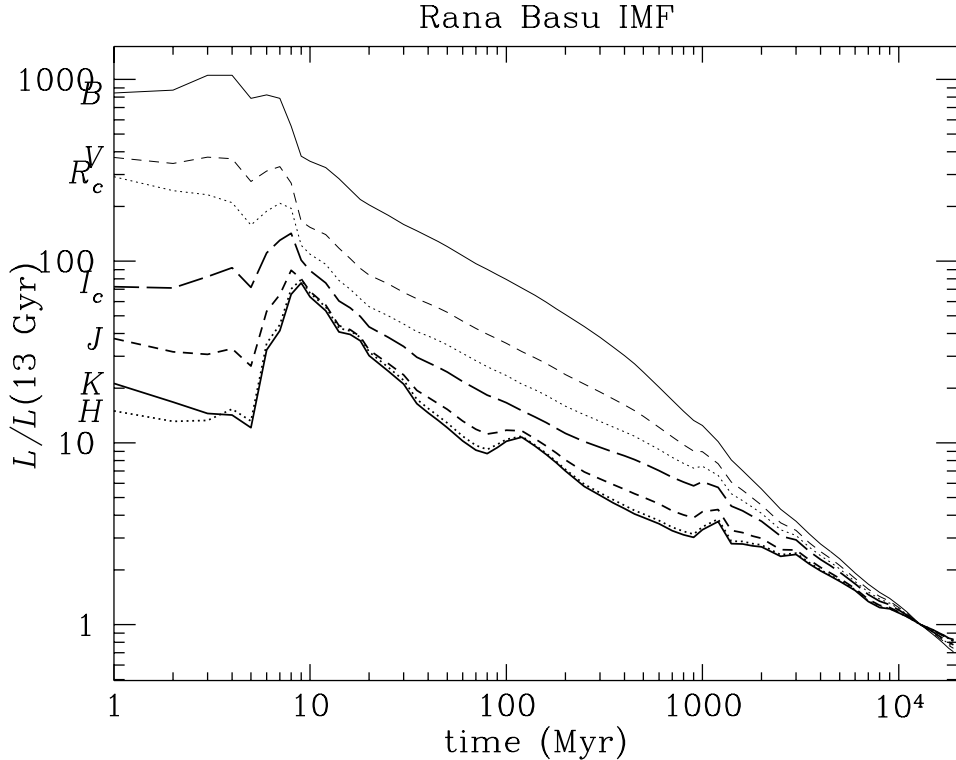


Figure 1: Time evolution of broad band luminosities (Johnson $BVJHK$ and Cousins RI) of stellar burst for stellar population with a Rana & Basu [26] IMF, using the *PEGASE* [14] spectral evolution model including nebular emission (which only affects the luminosities within 10 Myr from the burst).

U or far-UV, neither of which are plotted in Figure 1) and weakest in the H and K bands. Nevertheless, there is a burst of emission in H and K roughly 10 Myr after the starburst, when the massive stars evolve off the main-sequence to the giant branch. Table 1 below shows that the enhancement of broad band flux in the B band due to star formation occurring 1 Myr ago, relative to the B flux of an old stellar population of the same mass and IMF, is 40 times greater than the analogous enhancement of the K band flux.

Table 1: Broad-band luminosity enhancement relative to old (13 Gyr) population (normalized to the analogous K band relative enhancement)

Age	B	V	R_c	I_c	J	H	K
1 Myr	40	18	14	3.4	1.8	0.7	1
10 Myr	5.6	2.4	1.7	1.4	1.06	1.05	1
100 Myr	7.8	3.5	2.3	1.6	1.15	1.03	1
1 Gyr	3.7	2.7	2.4	1.9	1.26	1.04	1
2 Gyr	2.1	1.7	1.5	1.4	1.11	1.02	1

One interesting point is that the H band is to within a few percent as insensitive to recent star formation as the K band, and even less sensitive by up to 30% for very recent (< 5 Myr) star formation, with the inclusion of nebular emission in the adopted *PEGASE* [14] spectral evolution model, which is stronger in K because of free-free recombination enhancing the continuum at longer wavelengths. Another interesting point is that the J band at 1.25μ is almost

as insensitive to recent star formation as the K band, to within typically 20% or less, except for bursts younger than 8 Myr. The I_c band is considerably more sensitive to recent star formation than J (in Figure 1 and Table 1, I_c is typically three times more distant from K , logarithmically, than is J from K).

2 The DENIS survey

In December 1995, the DENIS (DEep Near Infrared Southern Sky Survey [12]) began imaging the southern sky, delimited by $-88^\circ \leq \delta \leq +2^\circ$, in the I_c ($0.8\ \mu\text{m}$), J , and K_s (K -short at $2.15\ \mu\text{m}$) wavebands. Its characteristics are given in Table 2 below. The data processing is done at the IAP (Paris) and Sterrewacht Leiden (Netherlands). The American 2MASS project [28] will have a similar scope, with slightly more sensitive J and considerably more sensitive K channels, and an H channel instead of our I channel.

Table 2: Characteristics of the DENIS survey (adapted from [12])

Institutions	Paris-Meudon, IAP, Leiden, Grenoble, Frascati, IAC, Innsbrück, Vienna, Lyon, Heidelberg, Budapest, Montpellier, Besançon, São Paolo
Declinations	$-88^\circ \leq \delta \leq +2^\circ$
Telescope	ESO 1m (fully dedicated)
Color bands	I ($0.8\ \mu\text{m}$), J ($1.25\ \mu\text{m}$), K_s ($2.15\ \mu\text{m}$)
Detectors	Tektronix CCD 1024 ² (I), Rockwell NICMOS-3 256 ² (JK)
Pixel size	$1''$ (I), $3''$ (JK dithered at $1''$)
Quantum efficiency	0.65 (I), 0.8 (J), 0.61 (K)
Exposure time	9 s (I), 8.8×1 s (JK)
Read-out noise	$7 e^-$ (I), $40 e^-$ (JK)
Observing mode	Stop & stare, concurrent 3-channel with dichroics
Scan geometry	$12'$ (RA) $\times 30^\circ$ (Dec)
Limiting magnitude (pt source 5σ)	18.0 (I), 16.0 (J), 13.5 (K)
Saturation magnitude	10.0 (I), 8.0 (J), 6.5 (K)
Survey period	December 1995 – mid 2000
Data	4000 GBytes (primary)
Cost	\$3 million

3 Extragalactic research and cosmology

A variety of scientific questions concerning extragalactic science and cosmology will be answered with the catalogs coming out of the DENIS and 2MASS databases:

Statistics of NIR properties of galaxies: DENIS and 2MASS will provide the first very large galaxy databases with NIR photometry, which should help for distance estimates of spiral galaxies with known velocity width (see [32]). Surface photometry of the brighter galaxies will be correlated with color as well as optical morphology, and with rotation velocity of known spirals [32] and used for distance estimates for ellipticals.

Cross-identification with other wavelengths: There will of course be plenty of cross-identification of DENIS and 2MASS galaxies with samples at other wavelengths, such as optical galaxy samples (see [32, 29]), IRAS galaxies, quasars, radio-galaxies, galaxies found in blind HI surveys, etc. The NIR properties (mainly their location in color-color diagrams) of such objects will be targeted for discovering new large samples of such objects. There will naturally be followups at non-NIR wavelengths of DENIS and 2MASS galaxies (see [30]).

Galaxy counts: From its *I*-band galaxy counts, DENIS should settle, once and for all, the debate on the bright-end of the galaxy counts, where first estimates [21] saw a depletion relative to the extrapolation of the faint-end counts, while later work [6] disputed this. At issue are the questions of galaxy evolution and whether the environment of the Local Group is underdense on very large scales ($z \lesssim 0.1$).

Zone of avoidance: Studying galaxies behind the Galactic Plane has two main applications (see [29]): 1) Mapping the large-scale distribution of galaxies in this still poorly known region. Indeed, the Zone of Avoidance contains interesting structures such as the largest large-scale concentration of matter in the local Universe, the Great Attractor (at the intersection of the Supergalactic Plane and the Galactic Plane [16]) and within the Great Attractor, the Norma cluster, Abell 3627, richer and closer than the Coma cluster [17]. 2) The fluxes and angular sizes of galaxies are affected by extinction from dust in the Galactic Plane, and one can measure this extinction from galaxy counts [8], colors [23], and color-color diagrams [29].

Structures of galaxies: Only a few catalogs of clusters [20, 10, 13] and compact groups [25] are based upon automatically selected galaxy samples, which happen to be optical and photographic (hence subject to photometric non-linearities). Because star formation is probably enhanced by galaxy interactions, one expects that the statistical properties of pairs, groups and clusters of galaxies built from NIR selected galaxy catalogs will be different from those built from optical catalogs. DENIS and 2MASS will thus have the double advantage of using an NIR galaxy sample based upon linear (non-photographic) photometry. The applications of such NIR-based samples of structures of galaxies are numerous [22] and include understanding the dynamics of these structures, their bias to projection effects, their constraints on Ω_0 and the primordial density fluctuation spectrum, their use as distance indicators, and the environmental influences on galaxies.

The large-scale structure of the Universe: The NIR selection and the linear photometry will also benefit the measurement of statistics (two-point and higher-order angular correlation functions, counts in cells, topological genus, etc.) of the large-scale distribution of galaxies in the Universe. For example, the (3D) primordial density fluctuation spectrum of galaxy clustering can be obtained from the two-point angular correlation function [2] or from the 2D power spectrum [3]. Moreover, by the end of DENIS and 2MASS, large-scale cosmological simulations with gas dynamics incorporated (thanks to which galaxies are properly identified) will provide adequate galaxy statistics in projection that will be compared with those obtained from the surveys, iterating over the cosmological input parameters of the simulations.

DENIS has already made contributions in stellar astronomy, with a new short scale length (2.3 kpc) and cutoff (15 kpc) of the Galactic disk [27] and the discovery of three candidate brown dwarfs [11], one of which ($\leq 0.065 M_\odot$ in Corvus) has been confirmed spectroscopically [31].

4 Galaxy extraction

The advent of first DENIS results in stellar astronomy highlights the difficulty of extracting galaxies from the DENIS images. Indeed, at the star/galaxy separation limits of the I band (which is the most sensitive, see § 6), there are 3 to 5 times more stars than galaxies at high galactic latitudes [19], and up to 10^4 times more in the Galactic Plane (with considerably less favorable ratios at brighter magnitudes, since galaxy counts rise faster than star counts). Whereas much of the science outlined in section § 3 requires galaxy samples that are complete and reliable (with few stars or optical defects misidentified as galaxies), such complete and reliable galaxy extraction is hindered by the current weaknesses in the DENIS camera:

- Low sensitivity in K caused by the thermal emission of the instrument
- Undersampled PSF in J and K (despite the dithering mentioned in Table 2)
- Large PSF in I (typically $2''$), caused in part by defocusing, coma and astigmatism of the camera
- Important PSF variations across the frames (10% to 50%) with the same causes plus optical misalignment
- Elongated PSFs near the frame edges
- Artifacts caused by readout electronics

In particular, the star/galaxy separation in the I band depends crucially on the accurate modeling of the PSF across the DENIS frames. An r.m.s. error of 5% on the FWHM of the PSF leads to a loss of 0.5 magnitude in the completeness limit of galaxy extraction at given reliability of star/galaxy separation [1].

4.1 Pipeline

We have worked on the images that were bias subtracted, flat-fielded, background subtracted, and bad pixel flagged with the software written by J. Borsenberger [7], who has also performed absolute astrometry by tying to a copy at the CDS in Strasbourg of the USNO-A1.0 [24] astrometric catalog obtained from PMM scans. One of us (G.A.M.) has implemented a preliminary galaxy pipeline with the following steps:

- Cosmic ray and bad pixel filtering
- Reading photometric zero-points and airmasses from relevant files
- Galaxy extraction using *SExtractor* [5], version 1.2b6a (including a neural-network based star/galaxy separation [4], whose input parameters are 8 isophotal areas, the maximum intensity and as a control parameter, the FWHM of the PSF), with detection and Kron photometry [18] parameters optimized from simulated images [1]
- Modeling of the variations of the object FWHMs across the frame (with a program written by M.T.)
- Star/galaxy separation using the updated PSF at the object position obtained from the modeling across the frame, using E. Bertin's *SExPlay2*

4.2 Photometric accuracy

Photometry is an important aspect in understanding the diagnostics of galaxy extraction and of most algorithms of classical (not based on neural networks) star/galaxy separation. We report here on the first measures of photometric accuracy of DENIS candidate galaxies, using objects

lying in the $2'$ overlaps of adjacent images. Figure 2 shows the differences in photometry on overlap objects that are likely to be galaxies. The photometric accuracy on a given individual

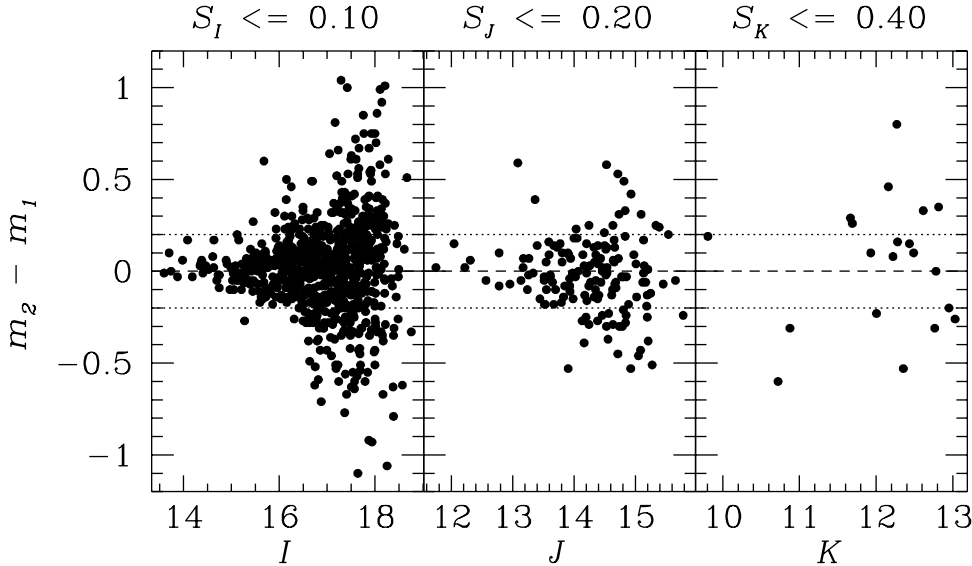


Figure 2: Photometric difference on overlap (concordant astrometry $< 2''$) candidate galaxies on 50 deg^2 , discounting flagged (blends, edge) objects and objects with centers within 20 pixels from edge of frames. The limiting neural network [5] stellarity index (0 for extended objects, 1 for stars) for galaxies is given at the top (PSF modeling was used, see § 4.3).

measurement is $\langle m_1 - m_2 \rangle_{\text{rms}}/2^{1/2}$. We thus infer from Figure 2 that $\sigma_I = 0.08$ at $I = 17$, $\sigma_J = 0.08$ at $J = 14.5$, and $\sigma_K = 0.42$ (0.31) at $K = 12$ (12.5). These do not include systematic photometric errors caused by uncertain zero-points, extrapolations to total magnitude, etc. The small number of overlaps in K means that the photometric accuracy in K is uncertain.

4.3 Star galaxy separation

The optical deficiencies of the DENIS camera cause variations of the PSF across the DENIS frames, which results in an excess of objects classified as extended (galaxies) in regions where the PSF is larger, if no modeling of the PSF is performed before star/galaxy separation [23]. One of us (M.T.) has modeled the PSF FWHM as a two-dimensional second order polynomial across the frame using unflagged objects with $I \leq 16.2$ and iteratively rejecting 2.5σ outliers (see also [7]).

Figure 3 shows how the neural network stellarity [5] seems to discriminate better between stars and galaxies once PSF modeling is incorporated, providing a gain of roughly one magnitude in the reliability limit (the DENIS strip 5544 used here spans galactic latitudes from 15° to 34° towards the Galactic Center).

Figure 4 shows the positions of candidate galaxies in the I band before and after modeling the PSF variations. Vignetting is apparent in both strips and corrected by the PSF modeling, perhaps too much so. Also, the upper left quadrant appears to produce an excess of galaxy

Figure 3: Neural network [5] stellarity parameter (1 = stellar, 0 = extended) versus magnitude for 180 frames of fairly low latitude strip 5544, without (*left*) and with (*right*) PSF modeling.

Figure 4: Positions of candidate galaxies ($I \leq 16.0$ and limiting neural network stellarity index for galaxies $S_I \leq 0.1$, only blending flags permitted) on DENIS frames, stacked over DENIS strips 5544 (*top*) and 5570 (*bottom*, $33^\circ \leq b \leq 61^\circ$), each containing 180 images. The *left* and *right* plots correspond to neural network stellarities defined without and with PSF modeling, respectively. Circle diameters vary as the square root of the fluxes.

candidates before PSF modeling, which may also be present after PSF modeling. However, the positions of the extended objects appear to lack uniform coverage of the frame in the PSF modeled star/galaxy separation. Hence, the PSF modeling is still imperfect and can probably be improved. We are currently analyzing new ways of modeling the PSF for adequate uniformity of the extracted galaxies.

One of us (W.B.) has obtained estimates of the reliability of star/galaxy separation through systematic visual inspection of 56 objects in one 6 deg^2 strip (5544), with $I \leq 16.0$ and who figure in the galaxy branch of the area-magnitude diagram shown in Figure 5. Borderline cases were checked visually by a second person (G.A.M.). 91% of objects passing both classical area vs. magnitude and neural network star/galaxy separation were confirmed as galaxies, while 7% were double stars (half of these were in an unusually dense region) and 2% (1 object) was an optical default (the spike of a mildly saturated star).

Figure 5: Area versus I magnitude for DENIS strip 5544 (objects at least 20 pixels from frame edges). *Circles* are candidate galaxies with stellarity $S_I \leq 0.10$, the *line* is a fiducial classical star/galaxy separation, and the *plus signs* above the line are classified as stars by the neural network ($S_I > 0.10$).

Similarly, we visually checked the 31 objects classified as stars by the neural network but situated above the classical dividing line in the area-magnitude diagram, and *all* were confirmed stars though 2 (6%) seemed to have faint galaxies superposed. For example, the isophotal area of the bright object at $I = 12$ classified as a star was seriously overestimated because it lied near a saturated star, but this did not fool the neural network.

5 Preliminary results on 50 deg²

There are two reasons to rely on I band star/galaxy separation when building lists of galaxies in J or K : 1) I is considerably more sensitive than J and K (except in highly extinguished regions, $A_V \gtrsim 6$ [29]), and 2) I has better angular resolution. Since typical $I - J$ colors are almost always bluer than 1.6 (see below), I band star/galaxy separation will be roughly 90% reliable (see § 4.3 above) down to $J = 16 - 1.6 = 14.4$ and for $K \lesssim 13.2$ (for similar reasons), well beyond the completeness limits for galaxy detection (see Table 3 below).

The results below are based upon I band star/galaxy separation using stellarity ($S_I \leq 0.10$) and area vs. magnitude (dividing line in Figure 5). Figure 6 presents the $I, I - J$ color-magnitude diagram for 8 high galactic latitude DENIS strips. The increased scatter at faint I magnitude is caused by photometric errors. The very blue and very red objects are probably misclassified stars. In any event, only the points above the two lines in Figure 6 have reliable star/galaxy separation. The galaxy locus seems to occur in the region $0.6 \leq I - J \leq 1.6$. At $J = 14.0$ (14.4), 96% (90%) of the galaxies have $I \leq 16.0$, so that this J list is over 87% (82%) reliable.

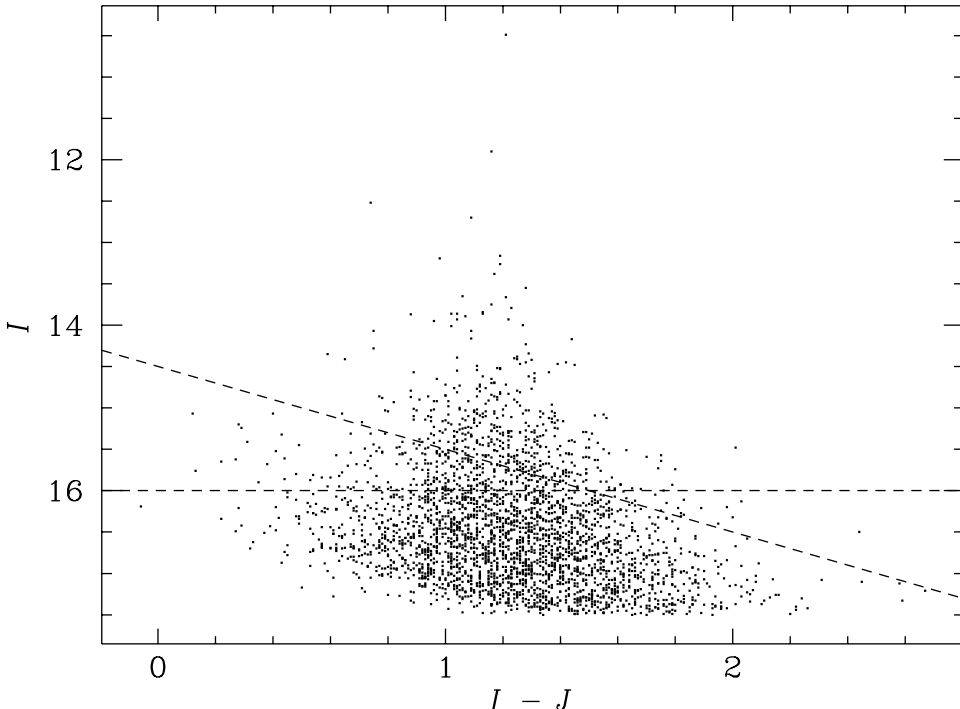


Figure 6: Color magnitude diagram for galaxies from 8 high latitude DENIS strips ($S_I \leq 0.1$ and isophotal area in I above critical line of Figure 5, with no additional star/galaxy separation in J ; objects closer than 50 pixels to the frame edges are excluded). The *horizontal line* represents $I = 16$ and the *tilted line* represents $J = 14.5$.

Note that the magnitudes in these plots are based upon Kron [18] photometry, which attempts to approximate the total magnitude of galaxies. Since, I is more sensitive than J , the Kron aperture radius is larger in I . We thus expect fixed aperture colors to appear slightly redder.

In figure 7, we show the IJK color-color diagram for our 8 high latitude strips. The galaxies with reliable photometry (*large filled circles* in Figure 7) cluster around $I - J \simeq 1.2$ and $J - K \simeq 1.1$, and an important part of the scatter is caused by photometric errors. Again,

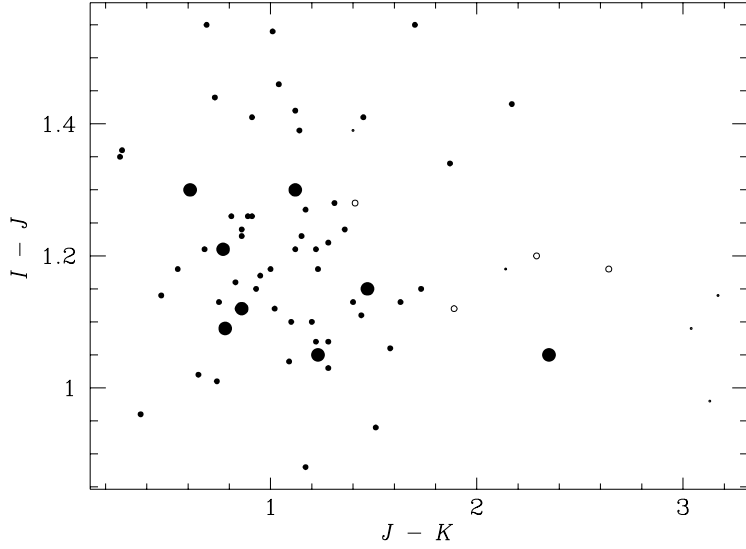


Figure 7: Color-color diagram for galaxies (using the same star/galaxy separation as in Figure 6 and no additional star/galaxy separation in K) in 8 high latitude DENIS strips. The *large circles* correspond to $I \leq 16.0$ and $K \leq 11.5$, the *small circles* to $I \leq 16.0$ and $K > 11.5$, the *dots* to $I > 16$. The *solid* and *open circles* correspond to $J \leq 14.4$ and $J > 14.4$, respectively.

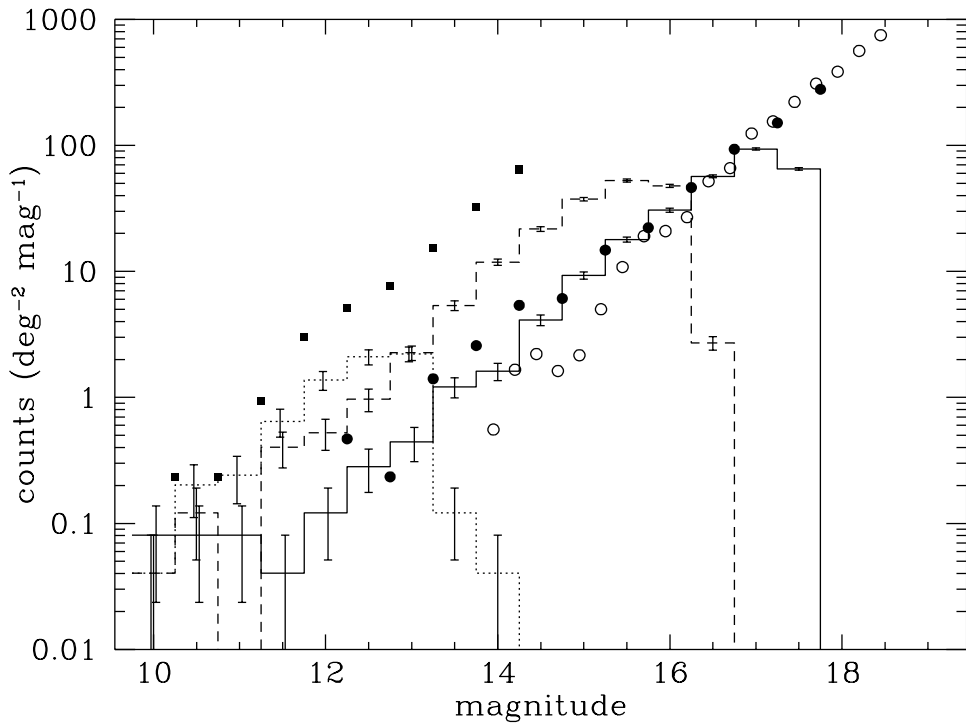


Figure 8: DENIS differential galaxy counts (using the same star/galaxy separation as in Figure 6, but with an additional color criterion deduced from Figure 6: $0.6 \leq I - J \leq 1.6$). Objects closer than 50 pixels to the frame edges are excluded, for a total equivalent area of 50 deg². The *dotted (left)*, *dashed (middle)*, and *solid (right)* *histograms* correspond to the DENIS counts in K , J , and I_c , respectively. Data points are counts from Gardner *et al.* [15] in K (*squares*) and I_c (*filled circles*) and from Lidman & Peterson [19] in I_c (*open circles*).

the colors within fixed apertures will be redder (see above). We are in the process of visualizing the galaxies that appear unusually red in $J - K$, but we note that most of these are too faint for very reliable star/galaxy separation in I and/or accurate photometry in J or K .

Figure 8 shows the galaxy counts in IJK bands for the 8 high galactic latitude DENIS strips. The DENIS I counts follow Gardner *et al.*'s [15] out to a 75% completeness limit of $I \simeq 17.25$. The disagreement at the bright end with Lidman & Peterson [19] argues for a *high bright-end normalization of galaxy counts* (see [6]), although not as high as Gardner *et al.*'s.

Note that DENIS, Gardner *et al.* and Lidman & Peterson all work with the Cousins I band, so no conversion was made from another I filter. Also, our survey has smaller error bars at the bright end as it covers 4 to 5 times the solid angle of the two cited surveys. In comparison with Gardner *et al.*'s [15] K counts, the DENIS K counts become incomplete at $K \simeq 11.25$. Figure 8 shows what we believe are the first reliable bright galaxy counts in J , and are roughly 80% (50%) complete out to $J \simeq 15.25$ (15.75). The J counts can be parameterized by $N(J) \simeq 11 \times \text{dex}[0.6(J - 14)] \text{ deg}^{-2} \text{ mag}^{-1}$.

6 Discussion

With the plots presented above, we are now in a position to provide our expected limits for the DENIS survey. From Table 3 below, we infer that star/galaxy separation is the limiting factor in I and J , while completeness and accurate (0.20 magnitude) photometry are the limiting factors in K . And from the counts of Figure 8, we estimate that complete, reliable, and

Table 3: Estimated DENIS limits from 50 deg^2 of reduced data

	I_c	J	K
completeness ($\simeq 80\%$)	17.25	15.25	11.25
star/galaxy separation (90% reliability, from I)	16.0	14.0	12.5
photometry (0.10 magnitude accuracy)	17.4	15.0	<11?

photometrically accurate DENIS catalogs will include 600 000, 200 000, and < 8000 galaxies at $I < 16.0$, $J < 14.0$, and $K < 11.2$, respectively. A cooling system has been very recently installed on the DENIS camera, and we hope that this will improve the K -band sensitivity. We also expect that better star/galaxy separation, in particular through better modeling of the PSF variations across the frames, will increase the reliability limit up to $I \simeq 16.5$, which will roughly double the number of galaxies in the complete and reliable I and J band catalogs.

Acknowledgements. We are grateful to P. Fouqué and the DENIS operations team for running the DENIS telescope, J. Borsenberger for developing the pre-extraction and astrometric calibration software necessary for the results presented here, E. Bertin for providing numerous updates to his *SExtractor* and *SExPlay2* software used for galaxy extraction and star/galaxy separation, and for comments on the manuscript, and M. Fioc for providing intermediate results from his *PEGASE* spectral evolution software.

References

- [1] Banchet V., 1998, PhD thesis, University of Paris 6, in preparation

- [2] Baugh C.M. & Efstathiou G., 1993, *MNRAS* **265**, 145
- [3] Baugh C.M. & Efstathiou G., 1994, *MNRAS* **267**, 323
- [4] Bertin E., 1995, PhD thesis, University of Paris 6
- [5] Bertin E. & Arnouts S., 1996, *Astr. Astrophys. Suppl. Ser.* **117**, 398
- [6] Bertin E. & Dennefeld M., 1997, *Astr. Astrophys.* **317**, 4
- [7] Borsenberger J., 1997, in *The Impact of Large-Scale Near-IR Surveys* p. 181, eds F. Garzón *et al.*, Kluwer
- [8] Burstein D. & Heiles C., 1982, *Astron. J.* **87**, 1165
- [9] Cardelli J.A., Clayton G.C. & Mathis J.S., 1989, *Astrophys. J.* **345**, 245
- [10] Dalton G.B., Efstathiou G., Maddox S.J. & Sutherland W.J., 1994, *Astrophys. J.* **390**, L1
- [11] Delfosse X., Forveille T. *et al.*, 1997, *Astr. Astrophys.*, submitted
- [12] Epcstein N. *et al.* (48 authors), 1997, *ESO Messenger*, **87**, 27
- [13] Escalera E. & MacGillivray H.T., 1995, *Astr. Astrophys.* **298**, 1
- [14] Fioc M. & Rocca-Volmerange B., 1997, *Astr. Astrophys.*, in press (astro-ph/9707017)
- [15] Gardner J.P., Sharples R.M., Carrasco B.E. & Frenk C.S., 1996, *MNRAS* **282**, L1
- [16] Kolatt T., Dekel A. & Lahav, O., 1995, *MNRAS* **275**, 797
- [17] Kraan-Korteweg R.C., Woudt P.A., Cayatte V., Fairall A.P., Balkowski C. & Henning P.A., 1995 *Nature*, **379**, 519
- [18] Kron R.G., 1980, *Astrophys. J. Suppl. Ser.* **43**, 305
- [19] Lidman C.E. & Peterson B.A., 1996, *MNRAS* **279**, 1357
- [20] Lumsden S.L., Nichol R.C., Collins C.A. & Guzzo L., 1992, *MNRAS* **258**, 1
- [21] Maddox S.J., Sutherland W.J., Efstathiou G., Loveday J. & Peterson B.A., 1990, *MNRAS* **247**, 1P
- [22] Mamon G.A., 1994, *Astrophys. & Sp. Sci.*, **217**, 237
- [23] Mamon G.A., Banchet V., Tricottet M. & Katz D., 1997, in *The Impact of Large-Scale Near-IR Surveys* p. 239, eds F. Garzón *et al.*, Kluwer (astro-ph/9608077)
- [24] Monet D., 1997, *Bull. A.A.S.*, **188**, 54.04
- [25] Prandoni I., Iovino A. & MacGillivray H.T., 1994, *Astron. J.* **107**, 1235
- [26] Rana N.C. & Basu S., 1992, *Astr. Astrophys.* **265**, 499
- [27] Ruphy S., Robin A.C., Epcstein N., Copet E., Bertin E., Fouqué P. & Guglielmo F. 1996, *Astr. Astrophys.* **313**, L21
- [28] Schneider S. *et al.*, in these proceedings
- [29] Schröder A., Kraan-Korteweg R.C., Mamon G.A. & Ruphy S., 1997, in these proceedings
- [30] Theureau G. *et al.*, in these proceedings
- [31] Tinney C.G., Delfosse X. & Forveille T. 1997, preprint (astro-ph/9707239)
- [32] Vauglin I. *et al.*, in these proceedings

This figure "avsm.gif" is available in "gif" format from:

<http://arXiv.org/ps/astro-ph/9711281v1>

This figure "svsm.gif" is available in "gif" format from:

<http://arXiv.org/ps/astro-ph/9711281v1>

This figure "xy.gif" is available in "gif" format from:

<http://arXiv.org/ps/astro-ph/9711281v1>